An Orientation Estimator for the Wheelchair's Caster Wheels

Félix Chénier, Pascal Bigras, Rachid Aissaoui

***Abstract*—Wheelchair ergometers are a highly valuable tool in the study of the biomechanics of manual wheelchair propulsion. However, current ergometers have some drawbacks that affect their level of realism. For example, the moment of inertia of the wheelchair-user system and the caster wheels' orientation are usually neglected, despite their high influence on the wheelchair's behavior. Taking these factors into account requires a complex dynamic model, and the calibration of such a model requires on-the-field recordings of the caster wheels' orientation, which are currently difficult to obtain. In this paper, we have proposed an open-loop observer that estimates each caster wheel's orientation (CWO) based only on the rear wheels' kinematics. The model was validated by propelling the wheelchair on three different floors (vinyl, carpet, and concrete) with five different normal forces between the caster wheels and the ground. Comparison between the estimated CWO and a reference one recorded by an optoelectronic device gave an accuracy error of less than $\pm 8^\circ$. This error reduced to $\pm 5^\circ$ when the wheelchair was propelled following straight or slightly curved patterns. This observer has implications in the design of better wheelchair ergometers and simulators, as well as in the control of electric wheelchairs.**

***Index Terms*—State estimation, Observers, Ergometers, Handicapped aids, Robot kinematics**

I. Introduction

Research in the design of manual wheelchairs has been growing actively since the last decade, which brings an extensive use of stationary ergometers. These ergometers aim to reproduce the dynamic behavior of a manual wheelchair and to record the biomechanical data representing real-life propulsion. As a matter of fact, fixing a wheelchair on a treadmill should represent highly realistic propulsion conditions [1]. However, the user cannot control his speed or change direction. Moreover, the strong effect of the floor material on the rolling resistance [2], [3], [4] cannot be replicated because the wheels are always on the same surface.

To overcome these limitations of fixed speed, direction, and kind of floor, a common solution is to place the rear wheels of the wheelchair on two separate rollers. Similarly, a complete system including the chair and both the wheels can be used. These ergometers are then tuned to approach the dynamic behavior given by Eq. (1) [5].

$$m\dot{v} = \sum F_{\text{app}} - F_{\text{air}}(v^2) - F_{\text{roll}}(v) - mg\sin\beta \qquad (1)$$

This project has received support from the National Sciences and Engineering Research Council of Canada (NSERC). There is no conflict of interest in this project.

Félix Chénier, Pascal Bigras and Rachid Aissaoui are with the Imaging and Orthopedics Research Laboratory, École de Technologie Supérieure de Montréal, 1100, rue Notre-Dame Ouest, Montréal, QC, H3C 1K3, Canada. Corresponding author: felix.chenier.1@ens.etsmtl.ca

where m is the total mass of the wheelchair-user system, v is the linear velocity, $\sum F_{\text{app}}$ is the sum of the applied forces on the wheels by the user, $F_{\text{air}}(v^2)$ is the air drag force, $F_{\text{roll}}(v)$ is the rolling resistance force caused by the deformation of the wheels on the ground, g is the gravitational acceleration, and β is the slope angle. Current ergometers generally distribute the inertial and resistive components of Eq. (1) equally on both the rear wheels, as given by Eq. (2).

$$\frac{m}{2} r_R \ddot{\theta}_i = F_{\text{app}i} - \frac{F_{\text{air}}(\dot{\theta}_i^2) + F_{\text{roll}}(\dot{\theta}_i) + mg\sin\beta}{2} \qquad (2)$$

where $\dot{\theta}_i$ is the angular velocity of wheel i, $F_{\text{app}i}$ is the tangential force applied on this wheel, and r_R is the radius of the wheels. Some ergometers approach this behavior by linking each wheel to a flywheel and a brake [6], [7], [8], [9], while others make use of motors [5], [10], [11] or a combination of flywheels, brakes, and motors [12].

The dynamic model expressed by Eq. (1) has two important advantages: first, it can be implemented with mechanical parts only. Second, it is relatively easy to calibrate the inertia and resistance of the wheels using the coast-down protocol [13]. However, it neglects some important aspects of the real wheelchair-user dynamics. First, it is valid for straight-line direction only, i.e. when turning, the axial moment of inertia of the wheelchair-user system is totally neglected. Second, the effect of each caster wheel's orientation (CWO) on the wheelchair motion is not taken into account, despite its important impact on the wheelchair's trajectory [14]. As both CWOs always change when executing turning maneuvers, we can conclude that no ergometer can adequately reproduce the dynamics of the wheelchair when the user is not wheeling strictly in a forward direction.

An ergometer aiming to reproduce the wheelchair propelled in a curvilinear direction must dynamically change the resistance felt by the user. For example, this resistance should be greater when the wheelchair's trajectory is not in line with the CWO. A motorized computer-controlled ergometer could achieve this task, provided that an adequate wheelchair dynamic model is used. Johnson and Aylor [15] developed such a theoretical model that adds three dynamic equations to Eq. (1); however, as many as six new parameters are required to express the dynamics of the CWO, such as the individual moment of inertia of each caster wheel, along with the sliding and rotating friction coefficients between the caster wheels and the ground. These parameters are difficult to measure experimentally and change for each ground surface, which prevent the direct application of this model to actual motorized ergometers.

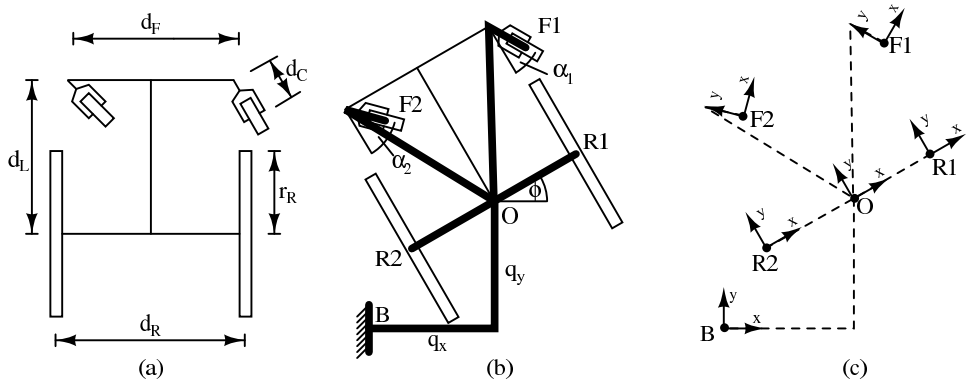

Fig. 1: Top view of the wheelchair. (a) Geometrical parameters. (b) Wheelchair expressed as a five degrees-of-freedom system: q_x, q_y (prismatic) ; ϕ, α_1, α_2 (revolute). (c) Reference frames used for the wheelchair model.

On the other hand, even if their model was simplified, it would still require real CWO recordings or estimations, in order to be fitted on real data [16]. The CWOs were measured only in a few studies, with the help of a dedicated caster wheel instrument [17]. No study known by the authors has focused on the estimation of these orientations without the use of cumbersome additional instrumentation.

In this paper, we have first expressed the dynamic behavior of the CWOs based only on the linear and angular speed of the wheelchair. No information on the floor surface or the inertial characteristics of the caster wheels is required. Subsequently, the stability of our model is developped to be used as a CWO estimator based on the recordings of the angular position of both the rear wheels. This information is readily available from instrumented wheels, such as SmartWheels [18]. Finally, the CWO is experimentally measured and estimated on multiple surfaces and with multiple normal forces between the ground, and the accuracy of the estimator is discussed based on the results from these experiments.

II. Mathematical model

While the caster wheels are often completely removed from the dynamic model of a wheeled vehicle, some authors have combined their effects into one single caster wheel [19], [20]. These three-wheeled models enable a constant contact between each wheel and the ground. However, as we were interested in the orientation of both the caster wheels, we included both in our model. The first implicit assumption was that at every moment, all four wheels are in contact with the ground. The second assumption was based on the common expression of the wheelchair as a nonholonomic vehicle with a rear wheels' lateral speed constrained to zero. As the generalization of this speed constraint to the front wheels is normally accepted [19], [20], our second assumption was that at all the time, none of the wheels is slipping laterally.

Figure 1 shows the kinematic model of the wheelchair expressed as a five degrees of freedom (d.o.f.) system composed of rigid bodies, where the non-slipping constraints of the wheels are temporarily not taken into account: these constraints will be introduced later. From Figure 1, we can determine the position of frame F1 relative to the base frame (B), expressed in the form of a generalized coordinate $\mathbf{p_{F1}} = [p_x \ p_y \ \phi_z]^T$

$$\mathbf{p_{F1}} = \begin{bmatrix} q_x + d_C s_{\phi\alpha_1} + (d_F/2)\, c_\phi - d_L s_\phi \\ q_y - d_C c_{\phi\alpha_1} + (d_F/2)\, s_\phi + d_L c_\phi \\ \phi + \alpha_1 \end{bmatrix}$$

where

$$s_\phi = \sin\phi \ ; \ s_{\phi\alpha_1} = \sin(\phi + \alpha_1)$$
$$c_\phi = \cos\phi \ ; \ c_{\phi\alpha_1} = \cos(\phi + \alpha_1)$$

and d_C, d_L and d_F are the geometrical parameters of the wheelchair.

The velocity of frame F1 relative to the ground (B) is obtained by time differentiation of $\mathbf{p_{F1}}$, and is expressed in the form $[v_x \ v_y \ \omega_z]^T$ [21]

$$\mathbf{v_{F1}} = \begin{bmatrix} \dot{q}_x + \left(d_C c_{\phi\alpha_1} - (d_F/2) s_\phi - d_L c_\phi\right)\dot{\phi} + d_C c_{\phi\alpha_1}\dot{\alpha}_1 \\ \dot{q}_y + \left(d_C s_{\phi\alpha_1} + (d_F/2) c_\phi - d_L s_\phi\right)\dot{\phi} + d_C s_{\phi\alpha_1}\dot{\alpha}_1 \\ \dot{\phi} + \dot{\alpha}_1 \end{bmatrix}$$

Generally, it is more useful to express the components of the velocity vector into the wheelchair's frame (O) rather than in the ground frame (B). Thus, we replaced the generalized speeds $\dot{q}_x$ and $\dot{q}_y$ with the speeds of the wheelchair, where $\dot{X}$ is the wheelchair's sliding speed in its right direction, and $\dot{Y}$ is as the wheelchair's rolling speed in its front direction. The transformation between both the reference frames is given by

$$\begin{bmatrix} \dot{q}_x \\ \dot{q}_y \end{bmatrix} = \begin{bmatrix} c_\phi & -s_\phi \\ s_\phi & c_\phi \end{bmatrix} \begin{bmatrix} \dot{X} \\ \dot{Y} \end{bmatrix}$$

and leads to

$$\mathbf{v_{F1}} = \begin{bmatrix} c_\phi \dot{X} - s_\phi \dot{Y} + \left(d_C c_{\phi\alpha_1} - \frac{d_F}{2} s_\phi - d_L c_\phi\right)\dot{\phi} + d_C c_{\phi\alpha_1}\dot{\alpha}_1 \\ s_\phi \dot{X} + c_\phi \dot{Y} + \left(d_C s_{\phi\alpha_1} + \frac{d_F}{2} c_\phi - d_L s_\phi\right)\dot{\phi} + d_C s_{\phi\alpha_1}\dot{\alpha}_1 \\ \dot{\phi} + \dot{\alpha}_1 \end{bmatrix}$$

This velocity is then projected into its own frame using

$${}^{\mathbf{F1}}\mathbf{v_{F1}} = \begin{bmatrix} c_{\phi\alpha_1} & s_{\phi\alpha_1} & 0 \\ -s_{\phi\alpha_1} & c_{\phi\alpha_1} & 0 \\ 0 & 0 & 1 \end{bmatrix} \mathbf{v_{F1}}$$

which leads to

$$
{}^{\mathbf{F1}}\mathbf{v}_{\mathbf{F1}} = \begin{bmatrix} c_{\alpha_1}\dot{X} + s_{\alpha_1}\dot{Y} + \left(d_C + (d_F/2)\, s_{\alpha_1} - d_L c_{\alpha_1}\right)\dot{\phi} + d_C\dot{\alpha}_1 \\ -s_{\alpha_1}\dot{X} + c_{\alpha_1}\dot{Y} + \left(d_L s_{\alpha_1} + (d_F/2)\, c_{\alpha_1}\right)\dot{\phi} \\ \dot{\phi} + \dot{\alpha}_1 \end{bmatrix} \tag{3}
$$

By employing the same approach for the other extremities, we get

$$
{}^{\mathbf{F2}}\mathbf{v}_{\mathbf{F2}} = \begin{bmatrix} c_{\alpha_2}\dot{X} + s_{\alpha_2}\dot{Y} + \left(d_C - (d_F/2)\, s_{\alpha_2} - d_L c_{\alpha_2}\right)\dot{\phi} + d_C\dot{\alpha}_2 \\ -s_{\alpha_2}\dot{X} + c_{\alpha_2}\dot{Y} + \left(d_L s_{\alpha_2} - (d_F/2)\, c_{\alpha_2}\right)\dot{\phi} \\ \dot{\phi} + \dot{\alpha}_2 \end{bmatrix} \tag{4}
$$

$$
{}^{\mathbf{R1}}\mathbf{v}_{\mathbf{R1}} = \begin{bmatrix} \dot{X} \\ \dot{Y} + d_R\dot{\phi}/2 \\ \dot{\phi} \end{bmatrix} \tag{5}
$$

$$
{}^{\mathbf{R2}}\mathbf{v}_{\mathbf{R2}} = \begin{bmatrix} \dot{X} \\ \dot{Y} - d_R\dot{\phi}/2 \\ \dot{\phi} \end{bmatrix} \tag{6}
$$

where

$$
\begin{aligned} s_{\alpha_1} &= \sin\alpha_1 \;;\; s_{\alpha_2} = \sin\alpha_2 \\ c_{\alpha_1} &= \cos\alpha_1 \;;\; c_{\alpha_2} = \cos\alpha_2 \end{aligned}
$$

The non-slipping assumption can now be applied for each wheel. As each wheel's speed will be null in its x-direction, the following speed constraints vector is obtained from each first row of Eqs. (3) to (6)

$$
\begin{bmatrix} c_{\alpha_1}\dot{X} + s_{\alpha_1}\dot{Y} + \left(d_C + \frac{d_F}{2}s_{\alpha_1} - d_L c_{\alpha_1}\right)\dot{\phi} + d_C\dot{\alpha}_1 \\ c_{\alpha_2}\dot{X} + s_{\alpha_2}\dot{Y} + \left(d_C - \frac{d_F}{2}s_{\alpha_2} - d_L c_{\alpha_2}\right)\dot{\phi} + d_C\dot{\alpha}_2 \\ \dot{X} \\ \dot{X} \end{bmatrix} = \mathbf{0}
$$

The first three rows of this vector are independent, and effectively reduce the number of generalized speeds from five ($\dot{X}$, $\dot{Y}$, $\dot{\phi}$, $\dot{\alpha}_1$, $\dot{\alpha}_2$) to two. As a result, the CWO rates ($\dot{\alpha}_1$ and $\dot{\alpha}_2$) can be expressed as functions of the wheelchair's linear and angular speeds ($\dot{Y}$ and $\dot{\phi}$)

$$
\dot{\alpha}_1 = \frac{\dot{\phi}}{d_C}\left(d_L\cos\alpha_1 - \frac{d_F\sin\alpha_1}{2} - d_C\right) - \frac{\dot{Y}}{d_C}\sin\alpha_1 \tag{7}
$$

$$
\dot{\alpha}_2 = \frac{\dot{\phi}}{d_C}\left(d_L\cos\alpha_2 + \frac{d_F\sin\alpha_2}{2} - d_C\right) - \frac{\dot{Y}}{d_C}\sin\alpha_2 \tag{8}
$$

It is possible to estimate both the CWOs by time-integrating Eqs. (7) and (8). Therefore, an open-loop observer can be obtained by replacing α_1, α_2 and their derivatives with their estimates

$$
\dot{\hat{\alpha}}_1 = \frac{\dot{\phi}}{d_C}\left(d_L\cos\hat{\alpha}_1 - \frac{d_F\sin\hat{\alpha}_1}{2} - d_C\right) - \frac{\dot{Y}}{d_C}\sin\hat{\alpha}_1 \tag{9}
$$

$$
\dot{\hat{\alpha}}_2 = \frac{\dot{\phi}}{d_C}\left(d_L\cos\hat{\alpha}_2 + \frac{d_F\sin\hat{\alpha}_2}{2} - d_C\right) - \frac{\dot{Y}}{d_C}\sin\hat{\alpha}_2 \tag{10}
$$

In general, a closed-loop observer would be superior in terms of stability and robustness [22]. However, as no direct link can be made between the available information ($\dot{Y}$ and $\dot{\phi}$) and the CWOs (α_1 and α_2), it is impossible to build a closed-loop observer without adding instrumentation which would give information on the CWOs. Therefore, an additional condition will be necessary to ensure the convergence of the open-loop observer. This condition will be presented in the following section.

III. Stability of the Estimator

To use the open-loop observer specified by Eqs. (9) and (10), it is necessary to ensure that the estimated CWO will converge to the real CWO. We will first address the stability of the $\hat{\alpha}_1$ observer, and subsequently, the same reasoning will be applied for the $\hat{\alpha}_2$ observer. First, we define $\tilde{\alpha}_1$ as the estimation error, which is the difference between the estimated CWO ($\hat{\alpha}_1$) and the real CWO (α_1)

$$
\tilde{\alpha}_1 = \hat{\alpha}_1 - \alpha_1 \tag{11}
$$

For the estimator to be stable, $\tilde{\alpha}_1$ has to converge to zero. The condition for this convergence is obtained by studying the local stability of the estimator using a linearization of $\dot{\hat{\alpha}}_1$ around the variable α_1 [23]. By definition

$$
f(\hat{\alpha}_1) \approx f(\alpha_1) + \left.\frac{df(\hat{\alpha}_1)}{d\hat{\alpha}_1}\right|_{\hat{\alpha}_1=\alpha_1} (\hat{\alpha}_1 - \alpha_1)
$$

Therefore, for $f(\hat{\alpha}_1) = \dot{\hat{\alpha}}_1$,

$$
(\dot{\hat{\alpha}}_1 - \dot{\alpha}_1) \approx \left.\frac{d(\dot{\hat{\alpha}}_1)}{d\hat{\alpha}_1}\right|_{\hat{\alpha}_1=\alpha_1} (\hat{\alpha}_1 - \alpha_1)
$$

where $\dfrac{d(\dot{\hat{\alpha}}_1)}{d\hat{\alpha}_1}$ is obtained by the differentiation of Eq. (9) relative to $\hat{\alpha}_1$. After replacing $(\hat{\alpha}_1 - \alpha_1)$ and $(\dot{\hat{\alpha}}_1 - \dot{\alpha}_1)$ by $\tilde{\alpha}_1$ and $\dot{\tilde{\alpha}}_1$ according to Eq. (11), the linear approximation of the error dynamics can be expressed as

$$
\dot{\tilde{\alpha}}_1 \approx -\left(\frac{\dot{Y}}{d_C}\cos\alpha_1 + \frac{\dot{\phi}}{d_C}(d_L\sin\alpha_1 + \frac{d_F}{2}\cos\alpha_1)\right)\tilde{\alpha}_1 \tag{12}
$$

It must be noted that from Eq. (3), the linear speed of the right caster wheel is defined by

$$
\begin{aligned} &\left[{}^{\mathbf{F1}}\mathbf{v}_{\mathbf{F1}}\right]_2 = \\ &-\dot{X}\sin\alpha_1 + \dot{Y}\cos\alpha_1 + \dot{\phi}\left(d_L\sin\alpha_1 + (d_F/2)\cos\alpha_1\right) \end{aligned}
$$

As $\dot{X}$ equals zero according to the non-slipping assumption, the error dynamics can be expressed as a function of the linear speed of the caster wheel

$$
\dot{\tilde{\alpha}}_1 \approx -\frac{\left[{}^{\mathbf{F1}}\mathbf{v}_{\mathbf{F1}}\right]_2\tilde{\alpha}_1}{d_C}
$$

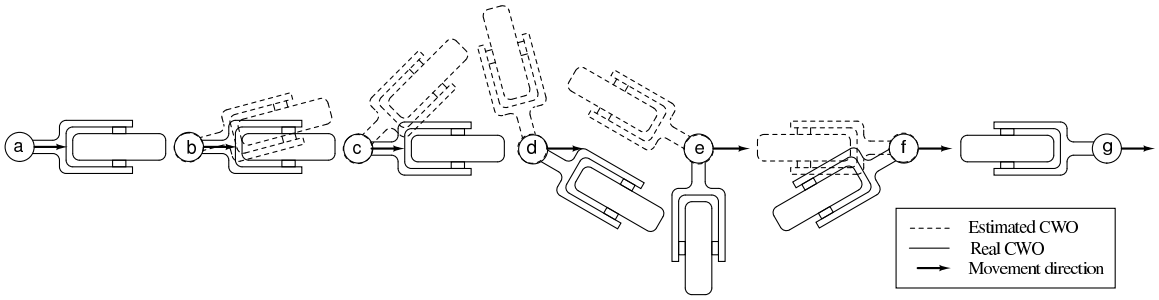

Fig. 2: An illustration of the estimator's possible behavior when the stability condition is ignored. In **a**, the wheelchair is propelled in such a way that the caster wheel is rolling completely backwards. This is an unstable situation and in **b**, a perturbation causes the estimator to deviate. We can see in **b** and **c** that as long as the caster wheel keeps rolling backwards, the estimator would eventually converge to 180° error. However, as the caster wheel is propelled in an unstable way, it starts to deviate in **d**, then its speed sign changes in **e**. From there, the stability condition is met and the estimation error converges back to 0°.

Following the same approach, we can obtain a similar equation for the left caster wheel, thus generalizing for the caster wheel i yields

$$\dot{\tilde{\alpha}}_i \approx -\frac{\left[{}^{\mathbf{Fi}}\mathbf{v}_{\mathbf{Fi}}\right]_2 \tilde{\alpha}_i}{d_C} \tag{13}$$

It is well known that the solution of this differential equation will converge to zero as $t \to \infty$ if and only if $\left[{}^{\mathbf{Fi}}\mathbf{v}_{\mathbf{Fi}}\right]_2$ is always greater than zero. A direct consequence of this conclusion is that to ensure the stability of the estimator, the caster wheel must be rolling forward.

It should also be noted that when the stability of the estimator is evaluated using the same approach but with a linearization around $\alpha_1 + 2k\pi$ for $k \in \mathbb{Z}$ instead of α_1, the error dynamics gives

$$\dot{\tilde{\alpha}}_i \approx -\frac{\left[{}^{\mathbf{Fi}}\mathbf{v}_{\mathbf{Fi}}\right]_2 (\tilde{\alpha}_i - 2k\pi)}{d_C}$$

which means that when the caster wheel is rolling forward, the estimation error $\tilde{\alpha}_i$ converges to any multiple of 2π depending on its initial condition. This is however not a problem, because an orientation error of $2k\pi$ is geometrically equivalent to no error.

Finally, a linearization around $\alpha_1 + (2k+1)\pi$, which corresponds to a 180° error, gives

$$\dot{\tilde{\alpha}}_i \approx \frac{\left[{}^{\mathbf{Fi}}\mathbf{v}_{\mathbf{Fi}}\right]_2 (\tilde{\alpha}_i - (2k+1)\pi)}{d_C}$$

which means the estimation error would converge to 180° as long as the caster wheel is rolling backwards. However, although this 180° error seems like a new stable point, it is not. This contradiction comes from the fact that the only way to negate $\left[{}^{\mathbf{Fi}}\mathbf{v}_{\mathbf{Fi}}\right]_2$ is by propelling the caster wheel in an unstable way. As a consequence, the error would indeed converge to 180° if the caster wheel was kept rolling backwards; however, this condition by itself is unstable as the caster wheel will tend to deviate. Figure 2 is an illustration of this behavior. Thus, it can be concluded that ignoring the estimator's stability condition will prevent the estimator to converge to the real CWO, but only temporarily, because the caster wheel will eventually change its orientation and make the estimator stable again.

From a practical point of view, the most obvious means to ensure the stability would be to install an anti-return mechanism on the caster wheels, which would block the wheels from rolling backwards. However, while this solution would certainly work, it is not always convenient. In fact, most standard wheelchairs do not have this type of add-on available. Moreover, the added friction would affect the dynamic characteristics of the wheelchair, which should be avoided in some applications, such as the characterization of the wheelchair-user dynamic model.

A more readily available solution would be to install an anti-return mechanism on the rear wheels. However, although it would work in most situations, we must show that if the rear wheels cannot roll backward, the caster wheels will not roll backward either, which is unfortunately false. A graphical counter-example is shown in Figure 3, where a sudden change in the wheelchair direction causes a brief instability. However, if the estimator has been stable for a while before this situation occurs, the error $\tilde{\alpha}$ can be assumed to be small, and this instability is unlikely to amplify the error enough to affect the overall estimate. In conclusion, an anti-return device on the rear wheels could minimize the cost and trouble inherent to the installation of the same device on the caster wheels, but extreme situations like this one should be avoided or at least monitored to keep the estimator as stable as possible.

IV. Experimental validation

The accuracy of the estimator was evaluated by comparing the estimated right CWO ($\hat{\alpha}_1$), computed from the angular position of each rear wheel, to a reference right CWO (α_1), measured by an optoelectronic device, for different test conditions.

A. Test conditions

In real-life conditions of manual wheelchair propulsion, the normal forces between the ground and the wheels continuously change because of the variation of the user's center of mass (COM) and the acceleration and deceleration of the

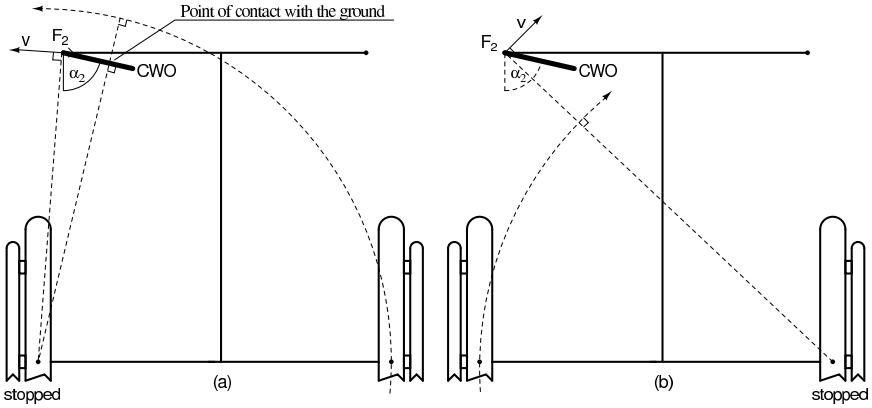

Fig. 3: Anti-return mechanism on the rear wheels: a case where the estimator becomes temporarily unstable. The rolling speed of the left caster wheel is obtained by projecting the vector v on the CWO (tick line), with v being the speed of point F_2 relative to the ground. When propelling the wheelchair while the left rear wheel is stopped (a), the CWO settles to the tick line. If immediately after, the right rear wheel is stopped and the left rear wheel is propelled (b), the projection of v on the CWO now points toward the caster wheel, which negates its rolling speed for a brief instant.

wheelchair-user system's COM [24]. As a consequence, the friction forces between the ground and the wheels may drop during a propulsion cycle, which could cause slipping of the wheels. Moreover, the friction coefficient between the ground and the wheels is highly dependant on the kind of floors [2], [3], [4]. As these variations of normal forces and friction coefficient could possibly affect the non-slipping assumption, the estimator was tested on three different kinds of floors that are commonly encountered in everyday life: vinyl, carpet, and concrete. For each kind of floors, five normal forces were applied on the caster wheels, starting from 443 N, which could simulate a normally weighted paraplegic man with 50% of his weight on the caster wheels [25]. This weight distribution corresponds to a seated user with a considerably flexed trunk. Subsequently, we decremented the load down to 63 N, which represents the extreme case where 100% of the subject's weight is on the rear wheels.

For each weight/floor combination, the instrumented wheelchair was pushed several times by an operator placed behind. At first, the wheelchair was pushed following straight to slightly curved patterns, with the right caster wheel's turning radius of at least 1 m. This simulated a propulsion in a large place such as a hall or corridor. Subsequently, the operator pushed the wheelchair following oscillatory patterns, with the right caster wheel's turning radius gradually decreasing from 1 to 0.2 m. This simulated the fast-changing CWO when the wheelchair is propelled in a tight space. To minimize the dynamic effects of the wheelchair's acceleration and deceleration on the normal ground forces, the operator kept the wheelchair's speed constant at $0,77 \pm 0,13$ m/s (mean ± s.d. computed from our experimental results) for the straight and slightly curved patterns, which corresponded to a commonly used speed [26]. For the oscillatory patterns, the wheelchair's frequency of oscillation was kept below 1 Hz, to match real-life conditions and to minimize the dynamic effects of the changes in the wheelchair's direction on the normal ground forces. During all the experiments, the operator looked at the right caster wheel to verify its constant contact with the ground. A release from the ground was noticed by the wheel ceasing to roll or keeping the same orientation while the wheelchair was changing direction.

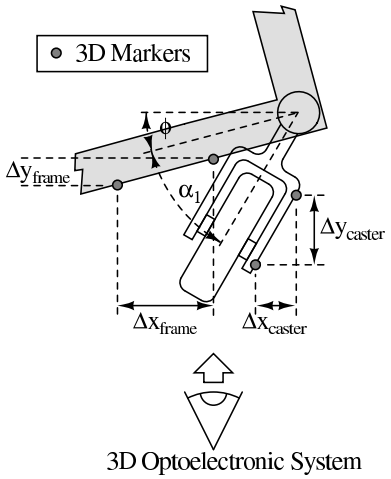

Fig. 4: Top view of the four infrared emitters mounted on the wheelchair frame and the caster fork.

B. Instrumentation

Two SmartWheels (3rivers Inc.) were mounted on a wheelchair (A4, Invacare Corp.) to collect the angular position of each wheel with a sampling frequency of 240 Hz. Additionally, four infrared emitters were placed on the wheelchair: two on the frame and two on the right caster wheel fork (Fig. 4). The 3D position of these emitters was acquired by a Visualeyez II VZ4000 tridimensional optoelectronic system (Phoenix Technologies Inc.) with a sampling frequency of 100Hz. To avoid hindering the wheelchair movements, the output from the SmartWheels were recorded by an external battery operated data logger (Anticyclone Systems AntiLog V4.0) and the optoelectronic system was operated in wireless mode.

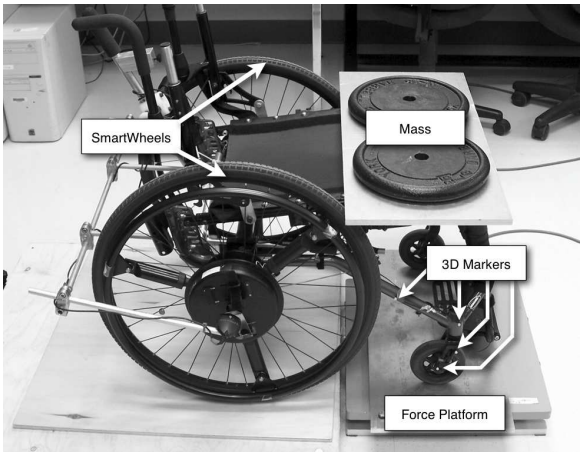

Fig. 5: Photo of the instrumented wheelchair placed on a scale prior to the experiment.

To measure the normal force between the caster wheels and the ground, the caster wheels were placed on a scale (AMTI OR6-7-1000 Force platform, Advanced Mechanical Technology Inc.) prior to the experiments, as shown in Figure 5. Each weighing was done with the caster wheels trailing backward. Measurement with different weight combinations gave the following normal forces: 63, 157, 251, 348 and 443 N.

C. Data processing

After recording and synchronizing the signals from the instrumented wheels and optoelectronic system, both the estimated CWO ($\hat{\alpha}_1$) and reference CWO (α_1) were computed.

The estimated CWO was obtained by first filtering the rear wheels' angular position θ_1 and θ_2 by $sG(s)$ in Laplace domain, to obtain the filtered angular speeds $\dot{\theta}_1$ and $\dot{\theta}_2$, where $G(s)$ is a low-pass Butterworth filter of order 6 with a cutoff frequency of 6 Hz. This frequency has been found to be the highest frequency of interest for manual wheelchair propulsion [27]. Based on these angular speeds, $\dot{Y}$ and $\dot{\phi}$ were calculated using Eqs. (14) and (15).

$$\dot{Y} = \frac{r_R(\dot{\theta}_1 + \dot{\theta}_2)}{2} \tag{14}$$

$$\dot{\phi} = \frac{r_R(\dot{\theta}_1 - \dot{\theta}_2)}{d_R} \tag{15}$$

The estimated CWO change rate ($\dot{\hat{\alpha}}_1$) was obtained from Eq. (9), whose integration using the ode45 Runge-Kutta method led to the estimated CWO $\hat{\alpha}_1$.

The reference CWO α_1 was calculated using Eqs. (16) and (17), according to Figure 4.

$$\phi = \arctan\left(\frac{\Delta y_{\text{frame}}}{\Delta x_{\text{frame}}}\right) \tag{16}$$

$$\alpha_1 = \arctan\left(\frac{\Delta y_{\text{caster}}}{\Delta x_{\text{caster}}}\right) - \phi \tag{17}$$

The samples for which at least one infrared emitter was not visible were removed from the data set. Finally, α_1 was filtered by $G(s)$ to match the attenuation and phase of $\hat{\alpha}_1$.

As the reference CWO was measured experimentally, it inevitably contained a noisy signal. To quantify this error, the RMS positioning uncertainty ε_x and ε_y was taken from the optoelectronic device's calibration data (both ± 0.47 mm) and was used to obtain the uncertainty ε_α on the reference CWO, using Eq. (18) [28].

$$\varepsilon_\alpha = \sqrt{\sum_{i=1}^{4}\left(\left(\frac{\delta\alpha_1}{\delta x_i}\right)^2 \varepsilon_x^2 + \left(\frac{\delta\alpha_1}{\delta y_i}\right)^2 \varepsilon_y^2\right)} \tag{18}$$

where (x_i, y_i) are the coordinates of marker i.

This function was computed from the collected data and led to a reference CWO uncertainty of around $\pm 2^\circ$.

V. Results

Figure 6 shows two samples of the experimental results. The parts where the reference CWO was not computed correspond to the moments when the wheelchair was brought back to its starting position: the 3D markers were then not in the field of view of the optoelectronic device. Figure 6(a) shows the case where the wheelchair was pushed following straight-line or slightly curved patterns, whereas Figure 6(b) shows the case where the wheelchair was pushed following oscillatory patterns. On some local minima and maxima of Figure 6(b), it can be observed that the error $\tilde{\alpha}_1$ is a bit higher when the CWO quickly changes. To quantify this error, the standard deviation of $\tilde{\alpha}_1$ was calculated for each normal force/floor combination. Figure 7 shows the double of the standard deviation for each combination, which is the maximal estimation error 95% of the time.

We can observe that for the case where the wheelchair was following straight or slightly curved patterns, the difference of accuracy between the 15 conditions is lower than the accuracy of the reference CWO. Therefore, we cannot correlate the accuracy of the estimator to the normal ground force or the kind of floor. However, we can state that for this non- or low-turning case, the estimator error is globally below 5°, 95% of the time. When the wheelchair is oscillating, which induces CWO variations, the accuracy particularly drops for the vinyl floor with the lowest normal force, and for the carpet with the highest normal force. These two particular cases will be discussed in section VI.

Finally, to verify the stability of the estimator, $\hat{\alpha}_1$ was calculated from seven different initial conditions (-60°, -45°, -30°, 0°, 30°, 45° and 60°) based on one of the collected data sets. Figure 8 shows the convergence of $\hat{\alpha}_1$: in all the cases, the error converged to zero in less than 1 s, which confirms the stability of the system for those seven initial conditions.

VI. Discussion

From Figure 7, it can be observed that the worst estimator accuracy is for the vinyl floor with the lowest normal force. To explain this low accuracy, we recall our first assumption that all wheels are always in contact with the ground. However, in this case, sometimes only three wheels were contacting the ground owing to the floor-level irregularities. This situation did not happen on the other floors: it may be hypothesized

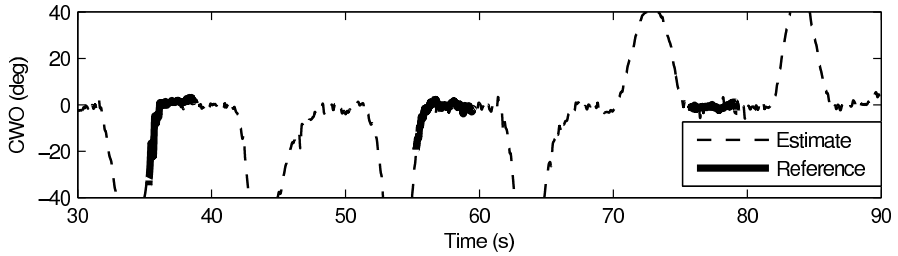

(a) The wheelchair was pushed following straight or slightly curved patterns.

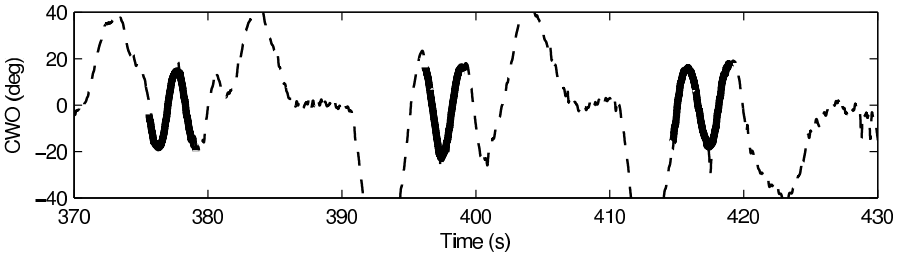

(b) The wheelchair was pushed following oscillatory patterns.

Fig. 6: Estimated CWO ($\hat{\alpha}_1$) and reference CWO (α_1) on the vinyl floor with a force of 251N between the ground and the caster wheels.

that this is because of their greater compliance (carpet) or roughness (concrete). We also believe that adding weight on the wheelchair deformed the tires enough to keep a constant contact, which is why we did not see this situation on the vinyl floor with other normal forces. Despite this violation of the first assumption, the error caused by the floor-level irregularities was not as pronounced when the wheelchair was not turning. This can be explained by the fact that for a straight pattern, the estimator predicts a steady-state CWO of 0°. By assuming that a caster wheel keeps its current orientation of 0° when it is released from the ground, the estimation remains valid even if the constant-contact assumption is violated, as long as the wheelchair is not turning.

The second lowest accuracy was found on the carpet with the maximal normal force. This is explained by an analysis of the friction between the wheels and the ground. It must be noted that the presented kinematic model is valid only if the caster wheels do not slip laterally. As the sliding friction coefficient cannot be infinite, the former condition can be fulfilled by a second requirement that the wheels are free to rotate. However, for a compliant floor and a high normal force, the caster wheel will tend to flatten and penetrate in the ground, thus becoming more difficult to rotate. Ultimately, the turning resistance leads to a lateral slipping of the wheel, which invalidates the second assumption. An exhaustive analysis of this phenomenon is presented in the Appendix. This explains the low accuracy for the particular case of the carpet, which is very compliant, when a high normal force is applied. Of course, this problem does not exist when the wheelchair is not turning, because the caster wheels do not rotate relative to the ground, and thus no turning resistive moment is generated.

The presented results show that, generally, the proposed CWO observer gives a good estimation of the caster wheels' orientation. However, some simplifications can limit its validity in some cases. First, this estimator does not consider the shimmy, which is a self-induced oscillating movement of the caster wheels started when the wheelchair speed reaches a certain threshold V_c [29]

$$V_c = \frac{d_C\sqrt{4M_F}}{\pi\Theta_0 I_w}$$

where d_C is the caster trail, M_F is the frictional moment between the caster wheel and the ground and is strongly related to the normal force applied on the caster wheel, Θ_0 is the initial angle between the CWO and the movement direction, and I_w is the caster wheel's moment of inertia. As most of the wheelchairs have a long caster trail to avoid this effect, we can assume that the caster wheels will not enter shimmy. This assumption was verified in our experiment.

Second, the reference CWO range was limited to around $\pm 30°$ by the use of an optoelectronic device: when the CWO was higher, the markers were not visible, thus, no reference CWO could be obtained. As a consequence, the accuracy of this estimator for CWOs higher than 30° could not be reported here.

Another limitation consists of the choice of an operator placed behind the wheelchair instead of a seated person propelling with the pushrims. This choice was made to control the normal force between the caster wheels and the ground. However, it may introduce an uncertainty when the normal force between the caster wheels and the ground is higher than 443 N, which is the highest normal force experimented. This case could happen when a heavy user terminates a propulsion cycle with his/her trunk completely flexed forward. We saw that such an augmentation of the normal force on a compliant floor would cause a loss of estimator's accuracy when executing turning maneuvers. This loss could not be evaluated owing to our experimental conditions. However, as this forward position is less common when turning, we believe that the presented experimental conditions give a good idea of

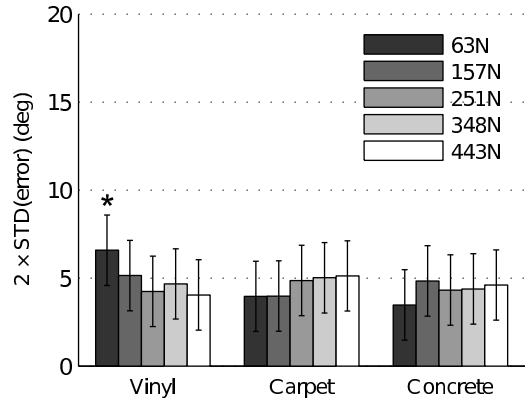

(a) Straight and slightly curved patterns

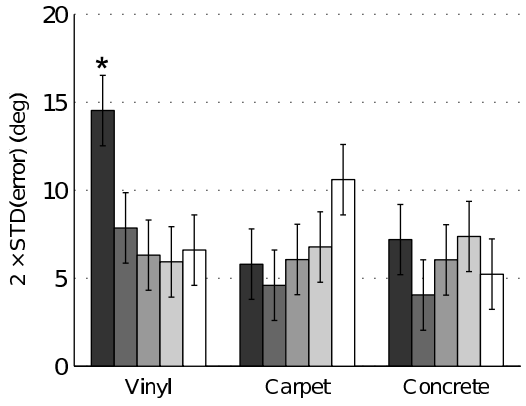

(b) Oscillatory patterns

Fig. 7: Accuracy of the estimator on different surfaces and with different normal forces on the caster wheels. The error bars correspond to the accuracy of the reference CWO, which is of about $\pm 2°$. The asterisk indicates that for this case, the caster wheel was not always in contact with the ground during the experiment.

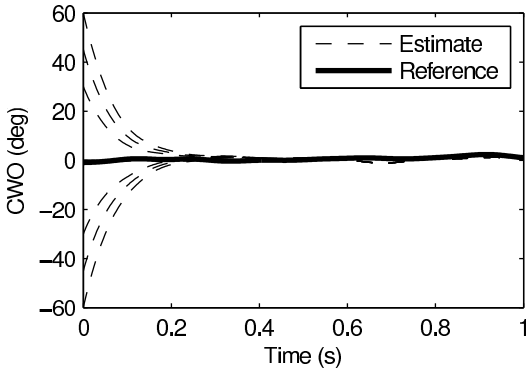

Fig. 8: Estimated CWO ($\hat{\alpha}_1$, thin line) and reference CWO (α_1, tick line) for different initial conditions : $\hat{\alpha}_1(0) \in \{-60°, -45°, -30°, 0°, 30°, 45°, 60°\}$

the real propulsion of a wheelchair. Finally, these experiments were performed on one specific wheelchair: while we are confident on the general conclusions of these experiments, it is hard to generalize the accuracy of the estimator for other wheelchairs, because the characteristics of the front wheels, such as their compliance and their materials may be different. Thus, future works with propulsion from real seated users on several wheelchairs should be carried out to definitely validate this estimator.

The applications of such an observer are numerous: the first example would be the characterization of the wheelchair-user dynamic model. In fact, as discussed in the introduction, the inclusion of the caster wheels' dynamics in the wheelchair-user model could be beneficial for the reproduction of a realistic aspect of the propulsion on an ergometer. Using the proposed observer, such a model could be fitted to real field data without needing to instrument the caster wheels. This new model could be programmed on a computer-controlled motorized ergometer [5], [10], [11], [12] to build an ergometer which would include the strong effect of the caster wheels on wheelchair propulsion.

Another direct application is in the control of powered wheelchairs. It was shown that the CWOs affect the direction of the wheelchair. For example, a powered wheelchair with a simple controller will deviate from its trajectory if the caster wheels are not originally oriented in the right direction [14]. Using our observer, the controller could be modified to take the CWOs into account and consequently modify its motor control, without any major modification to the wheelchair. Such a controller would be helpful for people who have serious interfacing limitations with their wheelchair [30].

VII. Conclusion

In this paper, we have presented the kinematic model of the wheelchair as a 5-d.o.f. robot. With the assumptions that all four wheels are continuously in contact with the ground and that none is slipping laterally, we reduced the number of generalized speeds from five to two. We then expressed the CWO rate as a function of both the rear wheels' speed. The time-integration of the CWO rate formed an open-loop observer that could estimate the CWO based on the rear wheels' speed. A stability analysis showed that the caster wheels must be rolling forward for this observer to be stable. Finally, the validity of this observer was verified by on-the-field measurements on different kinds of floors and with different normal forces between the caster wheels and the ground. This observer will be useful for the conception of a better dynamic model of the wheelchair-user system, which could lead to the design of more realistic wheelchair ergometers in the future.

Appendix

Analysis of the friction forces on a compliant floor

We begin by studying the forces acting on a caster-wheel assembly taken separately from the wheelchair (Fig. 9). The force F_x generated by the wheelchair frame generates a force and a moment at the center of the caster wheel, which is resisted by a friction force F_{Slide}, and a friction moment M_F.

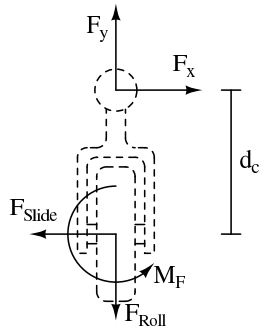

Fig. 9: Forces applied on the caster wheel. F_x and F_y result from the forces applied on the wheelchair whereas F_{Slide}, F_{Roll} and M_F are the sliding and rolling friction forces and the rotational moment of friction, respectively.

To apply the non-slipping assumption, there must be no lateral acceleration of the wheel; thus, $F_x = F_{\text{Slide}}$. Moreover, the wheel must be free to rotate along its vertical axis. As a consequence, when the wheel is rotating relative to the ground, the moment generated by F_x must be higher than or equal to the friction moment of the wheel: $d_c F_x \geq M_F$. Both these conditions yield Eq. (19), which ensures that the non-slipping assumption is considered in the case where the caster wheel is rotating relative to the ground.

$$F_{\text{Slide}} \geq \frac{M_F}{d_C} \tag{19}$$

If both the wheel and the floor were completely rigid, their contact would resolve to a single point and there would be logically no resistive moment. Consequently, Eq. (19) would always be respected. However, as neither the wheel nor the floor is rigid, it is necessary to evaluate F_{Slide} and M_F as acting on a patch rather than on a point. By using a Coulomb model of friction, the size of the patch has no effect on the sliding friction

$$F_{\text{Slide}} = \mu(N/2) \tag{20}$$

where μ is the friction coefficient between the ground and the wheel, and N is the normal force applied symmetrically on both the caster wheels.

However, for the rotational moment of friction, a patch size increase will also increase M_F. Johnson and Aylor [15] expressed the resistive moment on a circular patch with a constant normal forces distribution as

$$M_F = \frac{2}{3}\mu(N/2)r_P \tag{21}$$

where r_p is the radius of the contact patch. By substituting Eqs. (20) and (21) in Eq. (19), we can obtain an approximation of the non-slipping condition as a function of the normal force and the radius of the contact patch

$$\frac{\mu N}{2} \geq \frac{2\mu(N/2)r_P}{3d_C}$$

After simplification

$$\frac{2r_P}{3d_C} \leq 1 \tag{22}$$

It can be observed that if the contact patch is small, this inequality will always be respected and the non-slipping assumption will hold. However, if the contact patch grows substantially, this assumption may not be verified anymore. That said, the contact patch is bigger on the carpet than on the other floors because of the compliance of this floor. Additionally, it may be hypothesized that the contact patch will grow with an increase in the normal force N, because the wheel will deform and penetrate in the floor. The effect of this hypothesis can be observed in Figure (7), from which it can be concluded that Eq. (22) is violated for the highest normal force on the carpet.

Finally, it must be stated that Eq. (22) is a coarse approximation of the real non-slipping condition. In fact, the calculated sliding friction force would be valid only if all the infinitesimal parts of the contact patch were acting in the opposite direction of the sliding movement; in other words, if the only movement of the wheel was a sliding movement. Similarly, the calculated rotational moment of friction would be valid in the single case where the only movement of the wheel was a rotation relative to the ground. As both sliding and rotation occur simultaneously, there is a strong interdependency between F_{Slide} and M_F, which is not modelled here. Further studies should consider this interdependency. Notwithstanding this simplification, both F_{Slide} and M_F are overestimated, thus creating a non-negligible uncertainty in Eq. (22). In conclusion, this equation helps to explain the low accuracy for the highest normal force on the carpet, but should not be used to draw strong conclusions on the slipping of the caster wheels.

Nomenclature

d_R	Distance between both rear wheels
d_F	Distance between both front wheels
d_C	Caster trail
d_L	Length of the wheelchair
r_P	Radius of a circular contact patch between a caster wheel and the ground
r_R	Radius of the rear wheels
CWO	Caster Wheel's Orientation
α_1	Right CWO
α_2	Left CWO
θ_1	Right rear wheel's angular position
θ_2	Left rear wheel's angular position
ϕ	Axial angular position of the wheelchair relative to the ground
$\dot{Y}$	Linear speed of the wheelchair
$\dot{X}$	Sliding speed of the wheelchair
$\mathbf{v_a}$	Speed of reference frame **a** relative to the ground
${}^{\mathbf{b}}\mathbf{v_a}$	Speed of reference frame **a** relative to the ground, expressed in terms of frame **b** (notation from [21])

REFERENCES

[1] X. Martin, N. Tordi, M. Bougenot, and J. Rouillon, "Critical analysis of apparatus and evaluation methods for determination of physical capacity of spinal cord injured people using wheelchair," *Science and Sports*, vol. 17, no. 5, pp. 209–219, 2002.

[2] D. Chesney and P. Axelson, "Preliminary test method for the determination of surface firmness [wheelchair propulsion]," *IEEE Trans Rehabil Eng*, vol. 4, no. 3, pp. 182 – 7, Sept. 1996.

[3] A. M. Koontz, R. A. Cooper, M. L. Boninger, Y. Yang, B. G. Impink, and L. H. V. van der Woude, "A kinetic analysis of manual wheelchair propulsion during start-up on select indoor and outdoor surfaces.," *J Rehabil Res Dev*, vol. 42, no. 4, pp. 447–458, 2005.

[4] M. Hoffman, G. Millet, A. Hoch, and R. Candau, "Assessment of wheelchair drag resistance using a coasting deceleration technique," *Am J Phys Med Rehabil*, vol. 82, pp. 880 – 9, Nov 2003.

[5] R. Niesing, F. Eijskoot, R. Kranse, A. den Ouden, J. Storm, H. Veeger, L. van der Woude, and C. Snijders, "Computer-controlled wheelchair ergometer," *Med Biol Eng Comput*, vol. 28, no. 4, pp. 329–338, 1990.

[6] W. Langbein, C. Robinson, L. Kynast, and L. Fehr, "Calibration of a new wheelchair ergometer: the wheelchair aerobicfitness trainer," *IEEE Trans Neur Syst Rehabil*, vol. 1, no. 1, pp. 49–58, 1993.

[7] X. Devillard, P. Calmels, B. Sauvignet, A. Belli, C. Denis, C. Simard, and V. Gautheron, "Validation of a new ergometer adapted to all types of manual wheelchair.," *Eur J Appl Physiol*, vol. 85, no. 5, pp. 479–485, 2001.

[8] A. Faupin, P. Gorce, and A. Thevenon, "A wheelchair ergometer adaptable to the rear-wheel camber," *Int J Ind Ergon*, vol. 38, no. 7-8, pp. 601 – 7, 2008.

[9] F. Yao, *Measurement and Modeling of Wheelchair Propulsion Ability for People with Spinal Cord Injury*. PhD thesis, University of Canterbury, 2007.

[10] S. Shimada, R. Cooper, B. Lawrence, and R. Robertson, "Computer controlled wheelchair dynamometer," in *Proc of the 17th IEEE EMBS Annual Conference*, vol. 2, 1995.

[11] H. Yamada and T. Muto, "Using virtual reality to assess factors affecting shipboard accessibility for wheelchair users," *Control Intell. Syst.*, vol. 32, no. 1, pp. 52 – 7, 2004.

[12] C. Harrison, M. Grant, and B. Conway, "Haptic interfaces for wheelchair navigation in the built environment," *Presence: Teleoperators & Virtual Environments*, vol. 13, no. 5, pp. 520–534, 2004.

[13] C. DiGiovine, R. Cooper, and M. Dvornak, "Modeling and analysis of a manual wheelchair coast down protocol," in *Proc of the 19th IEEE EMBS Annual International Conference*, vol. 5, 1997.

[14] D. Ding, R. A. Cooper, S. Guo, and T. A. Corfman, "Analysis of driving backward in an electric-powered wheelchair," *IEEE Trans Control Syst Technol*, vol. 12, no. 6, pp. 934 – 943, 2004.

[15] B. W. Johnson and J. H. Aylor, "Dynamic modeling of an electric wheelchair," *IEEE Trans Industry Applicat*, vol. IA-21, no. 5, pp. 1284 – 1293, 1985.

[16] W. Khalil and E. Dombre, *Modeling, identification and control of robots*, ch. 12. Hermes, 1999.

[17] D. VanSickle, R. Cooper, J. Gonzalez, and M. Boninger, "Smarthub and smartcastor: force and moment sensing wheelchair wheels," in *Proc of the 19th IEEE EMBS Annual International Conference*, vol. 4, pp. 1871–1874 vol.4, Oct-2 Nov 1997.

[18] K. Asato, R. Cooper, R. Robertson, and J. Ster, "Smart wheels: development and testing of a system formeasuring manual wheelchair propulsion dynamics," *IEEE Trans Biomed Eng*, vol. 40, no. 12, pp. 1320–1324, 1993.

[19] Q. Yu and I. Chen, "A general approach to the dynamics of nonholonomic mobile manipulator systems," *J Dynamic Syst Meas Control*, vol. 124, p. 512, 2002.

[20] B. Bayle, J. Fourquet, and M. Renaud, "Manipulability of wheeled mobile manipulators: Application to motion generation," *Int J Robotics Research*, vol. 22, no. 7, pp. 565–582, 2003.

[21] J. Craig, *Introduction to robotics: mechanics and control*. Addison-Wesley Longman Publishing Co., Inc. Boston, MA, USA, 1989.

[22] P. Vas, *Parameter estimation, condition monitoring, and diagnosis of electrical machines*. Oxford University Press, USA, 1993.

[23] K. Ogata, *Modern control engineering*. Prentice-Hall, Inc. Upper Saddle River, NJ, USA, 1996.

[24] C. Sauret, P. Vaslin, M. Dabonneville, and M. Cid, "Drag force mechanical power during an actual propulsion cycle on a manual wheelchair," *IRBM*, pp. 3–9, 2008.

[25] Y. Dionyssiotis, K. Petropoulou, C. Rapidi, P. Papagelopoulos, N. Papaioannou, A. Galanos, and P. Papadaki, "Body composition in paraplegic men," *J Clin Densitom*, vol. 11, no. 3, pp. 437–443, 2008.

[26] M. Tolerico, D. Ding, R. Cooper, D. Spaeth, S. Fitzgerald, R. Cooper, A. Kelleher, and M. Boninger, "Assessing mobility characteristics and activity levels of manual wheelchair users," *J Rehabil Res Dev*, vol. 44, no. 4, p. 561, 2007.

[27] R. A. Cooper, C. P. DiGiovine, M. L. Boninger, S. D. Shimada, A. M. Koontz, and M. A. Baldwin, "Filter frequency selection for manual wheelchair biomechanics," *J Rehabil Res Dev*, vol. 39, no. 3, pp. 323 – 336, 2002.

[28] H. Coleman and W. Steele, *Experimentation and uncertainty analysis for engineers*. Wiley-Interscience, 1999.

[29] J. Kauzlarich, T. Bruning III, and J. Thacker, "Wheelchair caster shimmy ii: Damping," *J Rehabil Res Dev*, vol. 37, no. 3, pp. 305–313, 2000.

[30] T. Felzer and R. Nordmann, "Alternative wheelchair control," in *Proc of the 1st International IEEE-BAIS Symposium on Research on Assistive Technologies*, vol. 7, pp. 67–74, 2007.

Félix Chénier received B.Eng. and M.A.Sc. from the École Polytechnique de Montréal, Montréal, QC, Canada in 2006 and 2008 respectively, in electrical engineering. He is currently pursuing Ph.D. in health technologies at the École de Technologie Supérieure, Montreal, QC, Canada. His research interests are related to rehabilitation systems, robotics, simulation, and control.

Pascal Bigras received B.Eng. and M.Eng. in electrical engineering from the Department of Automated Manufacturing Engineering, École de Technologie Supérieure, University of Quebec, Montréal, Canada, in 1991 and 1993, respectively, and his Ph.D. in automatic control from the École Polytechnique de Montréal, in 1997. He is currently an Associate Professor with the Department of Automated Manufacturing Engineering. His research interests include nonlinear and robust control and their applications.

Rachid Aissaoui (M'98) received B.Sc. in electrical engineering from the University of Science and Technology of Oran, Oran, Algeria, in 1985, and his Ph.D. in biomechanics from the Université Joseph Fourier, Grenoble, France, in 1990. He joined the Clinical Research Institute of Montreal, QC, Canada, as the head of the Engineering Rehabilitation Team in 1991. He was responsible for the Gait Laboratory at the Sainte-Justine Hospital Research Center, Montreal, QC, Canada, from 1992 to 1995. He worked as a Researcher with the NSERC Industrial Research Chair on Wheelchair Seating Aids, Montreal, from 1996 to 2001. He is currently Professor at Ecole de Technologie Supérieure. His research interests are related to the 3D modeling of human locomotion, the development of tools for seating posture evaluation, and the dynamics of wheelchair propulsion. Dr. Aissaoui is a member of the CHUM, CRIR, REPAR, and the IEEE-EMB Society.